






Article

Thermal Stability and Kinetics of Degradation of Moxonidine as Pure Ingredient vs. Pharmaceutical Formulation

Bianca Baul¹, Adriana Ledeti^{2,*}, Denisa Cîrcioaban², Amalia Ridichie^{1,2}, Titus Vlase³, Gabriela Vlase³, Francisc Peter^{1,4,*} and Ionuț Ledeti^{1,2}

¹ Faculty of Industrial Chemistry and Environmental Engineering, University Politehnica Timisoara, 2 Victoriei Square, 300006 Timisoara, Romania; bianca.baul@student.upt.ro (B.B.); amalia-ioana.ridichie@student.upt.ro (A.R.); ionut.ledeti@umft.ro (I.L.)

² Advanced Instrumental Screening Center, Faculty of Pharmacy, Victor Babeș University of Medicine and Pharmacy, 2 Eftimie Murgu Square, 300041 Timisoara, Romania; circioaban.denisa@umft.ro

³ Research Centre for Thermal Analysis in Environmental Problems, West University of Timisoara, Pestalozzi Street 16, 300115 Timisoara, Romania; titus.vlase@e-uvt.ro (T.V.); gabriela.vlase@e-uvt.ro (G.V.)

⁴ Research Institute for Renewable Energy, University Politehnica Timisoara, 138 Gavril Musicescu, 300501 Timisoara, Romania

* Correspondence: afulias@umft.ro (A.L.); francisc.peter@upt.ro (F.P.)

Abstract: The stability of active pharmaceutical ingredients (APIs) and the corresponding pharmaceutical formulations are nowadays of great importance in pharmaceutical research and technology. The quality of an API or of finished pharmaceutical products (FPPs) is time dependent under the influence of several parameters, such as light and air exposure, temperature, and humidity. Additionally, the stability profile of an API is influenced by the formulation composition, due to the presence of excipients or by the characteristic of the packaging materials. In this sense, the main objective of this study was to analyze the degradation kinetics of the antihypertensive drug moxonidine as a pure ingredient (MOX) and in two different solid mixtures, one corresponding to a pharmaceutical formulation (MOXTAB) and the other to an enriched pharmaceutical formulation in MOX (MOXMIX). As investigation techniques, FTIR (Fourier transform infrared) spectroscopy and TG/DTG/HF analysis were employed, while the thermoanalytical data were processed according to the ASTM E698 kinetic method and the isoconversional methods of Flynn–Wall–Ozawa (FWO) and Friedman (FR). The kinetic methods revealed that the excipients have a stabilizing effect on MOX (in terms of E_a values), but the decomposition mechanism of the samples is complex, according to the results suggested by the analysis of E_a vs. α values.

Keywords: moxonidine; thermal stability; kinetic study; isoconversional methods; drug degradation



Citation: Baul, B.; Ledeti, A.; Cîrcioaban, D.; Ridichie, A.; Vlase, T.; Vlase, G.; Peter, F.; Ledeti, I. Thermal Stability and Kinetics of Degradation of Moxonidine as Pure Ingredient vs. Pharmaceutical Formulation.

Processes **2023**, *11*, 1738. <https://doi.org/10.3390/pr11061738>

Academic Editors: Alina Pyka-Pajak and Roberto Pisano

Received: 9 May 2023

Revised: 29 May 2023

Accepted: 31 May 2023

Published: 7 June 2023



Copyright: © 2023 by the authors. Licensee MDPI, Basel, Switzerland. This article is an open access article distributed under the terms and conditions of the Creative Commons Attribution (CC BY) license (<https://creativecommons.org/licenses/by/4.0/>).

1. Introduction

In the medical–pharmaceutical domain, the increasing percentage of patients with both obesity and hypertension led to the need to investigate molecules with therapeutic effects on these two chronic diseases [1]. From a physiological point of view, both conditions are associated with a hyperactivity of the sympathetic nervous system, including catecholamines and neuropeptides (leptin and neuropeptide Y) [2,3].

Moxonidine (abbreviated MOX, structural formula presented in Figure 1) is a new-generation API used in the treatment of mild to moderate essential hypertension [4], especially in overweight and obese patients [5], since it has been proved that the drug reduces body weight. The antihypertensive agent, along with rilmenidine, belongs to the second generation of the imidazoline derivatives, which are described as APIs with reduced sedative and central nervous system depressant activity and lower affinity to the α_2 -receptors compared to the first generation. The molecule acts as an agonist for the I1-imidazoline and α_2 -adrenergic receptors, participating in cardiovascular control by

reducing the sympathetic activity [6,7]. The pharmaceutical market currently provides three common pharmaceutical formulations along other generics: Physiotens[®], Moxon[®], and Cynt[®], with different concentrations of moxonidine—0.2 mg, 0.3 mg, and 0.4 mg, respectively, designed for oral administration as coated tablets. Currently, MOX is also being investigated for its efficacy in attention deficit hyperactivity disorder (ADHD), showing significant improvement in the symptoms [8].

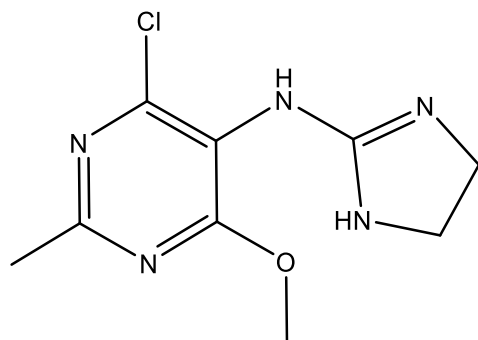


Figure 1. Chemical structure of moxonidine (4-chloro-N-(4,5-dihydro-1H-imidazol-2-yl)-6-methoxy-2-methylpyrimidin-5-amine).

Pharmaceutical formulations are obtained by conditioning APIs along excipients, which have a significant impact on the biopharmaceutical profile of the drug molecule [9]. The stability of the drugs can be evaluated using thermoanalytical tools, which lead to crucial information on its stability under thermal stress and decomposition under different conditions (in non-isothermal and/or isothermal conditions), based on irreversible mass loss [10] and phase transitions, including polymorphic shift [11]. Additionally, in the field of pharmaceuticals, thermal analysis can provide essential data on interactions between APIs and excipients [12,13], the formation and stability of supramolecular adducts such as guest–host complexes with cyclodextrins [14–17], salts and cocrystals [18–22], or even semisolid formulations, such as medicated jellies [23] or gels [24].

Kinetic analysis represents an analytical method based on the data obtained from various thermal analysis techniques (thermogravimetry and differential scanning calorimetry) and it serves as an important investigational method in the pharmaceutical research [10,25–27], among other scientific fields [28–30], leading to crucial information on stability, degradation mechanisms of the investigated compounds, and even shelf-life.

Considering the lack of information about the thermolysis mechanism for most substances currently used in therapy, isoconversional methods can be employed to determine their decomposition mechanism. This approach allows the approximation of the activation energy (E_a) without knowing or assuming an explicit model for the differential or integral conversion functions. To increase the quality of these studies, several recommendations have been described by the International Confederation for Thermal Analysis and Calorimetry (ICTAC) Kinetics Committee that must be taken into account in order to obtain realistic data [31–34].

The FWO integral isoconversional method is a fairly simple and widely used method to determine the value of the activation energy (E_a) of a decomposition process, using the data collected from the thermogravimetric curve (TG). The FWO method is based on the assumption that the conversion function does not fluctuate with the modification of the heating rate for all values of the conversion degree and it acts according to the Arrhenius-type temperature dependence without changing the form of the kinetic equation [35,36].

Using the FR differential isoconversional method, the values of the activation energies tend to be slightly higher than the ones determined with the FWO method; those results can be attributed to the calculation of the reaction rate and the higher sensitivity of the FR method to the experimental noise, due to differential processing of the data. Nonetheless,

the FWO and FR methods reveal the same tendency of variation for the values of the activation energies; as the conversion rate increases, so does the activation energy [35,37].

Searching the literature data regarding the physicochemical characterization of MOX by instrumental analysis, scarce information was obtained. In 2006, a study regarding the determination of MOX in the blood plasma of humans by liquid chromatography–electrospray ionization–mass spectrometry was conducted by Zhao, Ding, and Wei [38], followed by some other dedicated papers regarding the investigation of this compound and its impurities by chromatographic techniques [39–43].

Forced degradation studies were performed for MOX as pure API and in pharmaceutical formulations according to the International Conference for Harmonization guides in acid, neutral, and basic environments, as well as to oxidative, thermal, and photolytic decomposition, in both solution and solid state [41].

The paper of Allada et al. presents the preparation, characterization, and crystal structure determination of a novel salt containing MOX, namely, the hydrated saccharinate with improved water solubility, which was characterized by TGA (thermogravimetric analysis), DSC (differential scanning calorimetry), and XRPD (X-ray powder diffraction) [44].

To the best of our knowledge, there are no published reports on the thermal degradation of MOX in solid state under thermal stress, or on the investigation of the degradation process using isoconversional kinetic studies. Thus, this study is focused on the thermal stability characterization of the MOX during thermal stress in oxidative atmosphere, in pure form, as a commercialized formulation MOXTABB that contains 0.4 mg MOX/tablet, and as a 5:1 mixture of MOXTAB and pure MOX (abbreviated MOXMIX). The obtained experimental data were initially processed using the preliminary ASTM E698 kinetic method, followed by the isoconversional methods of FWO and FR. All compounds were also subjected to FTIR analysis in order to prove the identity and purity of the active ingredient (MOX), as well as the presence of this API in the complex samples (MOXTAB and MOXMIX).

2. Materials and Methods

2.1. Samples and Preparation

Moxonidine (MOX) was acquired from Sigma-Aldrich (St. Louis, MO, USA) and the purity was according to the European Pharmacopoeia (EP) Reference Standard. The sample was kept in a sealed vial according to the supplier's recommendations and was used in the studies as received.

The tablets were a commercialized product containing 0.4 mg MOX/dose, namely, Physiotens 0.4 mg (batch 28TACWG71H), produced by Mylan laboratories SAS/Viatis—France. In this study, 10 tablets were used. The excipients of the tablets were hydrated lactose, povidone K25, crospovidone, and magnesium stearate, as indicated in the patient information leaflet. The average mass of the tablet was 108.22 ± 1.11 mg, while after manually removing the film using a scalpel, the average mass was 93.91 ± 1.18 mg. The mass of the core taken into analysis was not the absolute mass of the core, but the remaining mass after the entire coating was removed together with some small external parts of the core.

Since MOXTAB contains 0.4 mg of MOX per tablet, we prepared a model system that mimics the behavior of the API in the commercialized formulation by adding to the crushed tablet (after mechanically removing the film) a required amount of API so that the final mixture contained one part of API to five parts of excipients. For this, 10 tablets were used; their film was completely removed by scratching and they were immediately crushed and triturated in an agate mortar, then sieved. Then, 100 mg of sieved powder was mixed with 20 mg of MOX using the agate mortar and then kept in sealed vials until analysis. The procedure was repeated in triplicate and the samples were in comparison, leading to practically identical results.

2.2. FTIR Investigations

FTIR spectra were drawn up using a Perkin Elmer SPECTRUM 100 device (Perkin-Elmer Applied Biosystems, Foster City, CA, USA) without any a priori preparation of the samples. Data were collected in a $4000\text{--}650\text{ cm}^{-1}$ domain on a UATR (Universal Attenuated Total Reflectance) accessory in order to eliminate the effect of pelleting due to the use of KBr and pressure. Spectra were built up after 64 co-added scans. The spectral range $2300\text{--}1900\text{ cm}^{-1}$ represents the crystal noise signal and has no spectroscopic significance.

2.3. Thermoanalytical Investigations

Thermal analysis investigations were carried out on a Perkin-Elmer DIAMOND apparatus (Perkin-Elmer Applied Biosystems, Foster City, CA, USA) to simultaneously obtain the TG (thermogravimetric/mass curve), DTG (derivative thermogravimetric/mass derivative), and HF (heat flow curve) in dynamic air atmosphere ($100\text{ mL}\cdot\text{min}^{-1}$) using open aluminum crucibles. The analyses were carried out under non-isothermal conditions at four heating rates β , namely, 5, 7, 10, and $15\text{ }^{\circ}\text{C}\cdot\text{min}^{-1}$, from ambient temperature up to $400/500\text{ }^{\circ}\text{C}$. To determine the thermal effects, the differential thermal analysis (DTA) data (in μV) were converted into HF (Heat Flow) data (in mW). The HF data (mW) were converted into normalized HF data by dividing the signal by the mass of the sample, thus obtaining the differential scanning calorimetry (DSC) data (in $\text{mW}\cdot\text{mg}^{-1}$).

2.4. Kinetic Study

The kinetic processing of the data (ASTM E698, Friedman and Flynn–Wall–Ozawa methods) was carried out on the first decomposition process of MOX, MOXTAB, and MOXMIX, using the AKTS—Thermokinetics Software version 4.46 (AKTS AG TechnoArk, Siders, Switzerland). As for abbreviations, we used the notations that are generally accepted by the ICTAC committee [34,45]: α —conversion degree, t —time, β —linear heating rate ($^{\circ}\text{C}\cdot\text{min}^{-1}$), A —pre-exponential factor according to kinetic model of Arrhenius (min^{-1}), $f(\alpha)$ —the differential conversion function, $g(\alpha)$ —the integral conversion function, E_a —activation energy ($\text{kJ}\cdot\text{mol}^{-1}$), R —universal gas constant ($\text{J}\cdot\text{mol}^{-1}\cdot\text{K}^{-1}$), T —absolute temperature (K), m_0 —mass of the sample at the beginning of decomposition, m_f —mass of the sample at the end of decomposition, m_T —mass of the sample at a certain temperature T .

3. Results and Discussion

3.1. FTIR Investigations

FTIR analysis was performed for all three samples, namely, pure MOX, the commercially available pharmaceutical formulation MOXTAB containing 0.4 mg MOX in each film-coated tablet and, MOXMIX (the 5:1 mixture of MOXTAB and MOX), in order to characterize the pure API and to identify its presence in both mixtures.

The obtained FTIR spectra are presented superimposed in Figure 2. The major characteristic bands [46–48] associated with pure MOX can be easily observed in the spectrum and the data are in accordance with the scientific literature [44]. As such, for the primary amine groups, the N–H stretching vibration is revealed by the band seen in the high wavenumber range ($3300\text{--}3125\text{ cm}^{-1}$) with a maximum at 3187 cm^{-1} . This value is slightly lower than the usual position of this type of vibration, the shift being most likely due to the formation of hydrogen bonds. The bending vibration of the N–H bond is associated with the peak seen at 1648 cm^{-1} , while the stretching vibrations of the different C–N bonds found within the architectural structure of the molecule can be correlated with the signals seen at 1219 and 1181 cm^{-1} . The stretching vibrations of the double C=N bonds present in the pyrimidine and 2-imidazoline heterocycles can be matched with the peaks seen at 1561 and 1524 cm^{-1} . The existence of the ether bond within MOX's structure can easily be related to the absorption band observed at 1092 cm^{-1} , since the C–O bond forms a C–O–C linkage whose stretching vibration determines a strong signal. At 857 cm^{-1} , a peak can be distinguished, most likely indicating the presence of the C–Cl bond. The remaining

hydrocarbon skeleton presents a series of characteristic vibrations, namely, the symmetric and asymmetric stretching vibrations of the C–H bonds from the methyl and methylene moieties (2997 , 2953 , and 2856 cm^{-1}), the bending vibrations of the $-\text{CH}_3$ groups (1469 and 1369 cm^{-1}), as well as the scissoring (1426 cm^{-1}), wagging (1313 cm^{-1}), and rocking (705) vibrations of the $-\text{CH}_2$ groups.

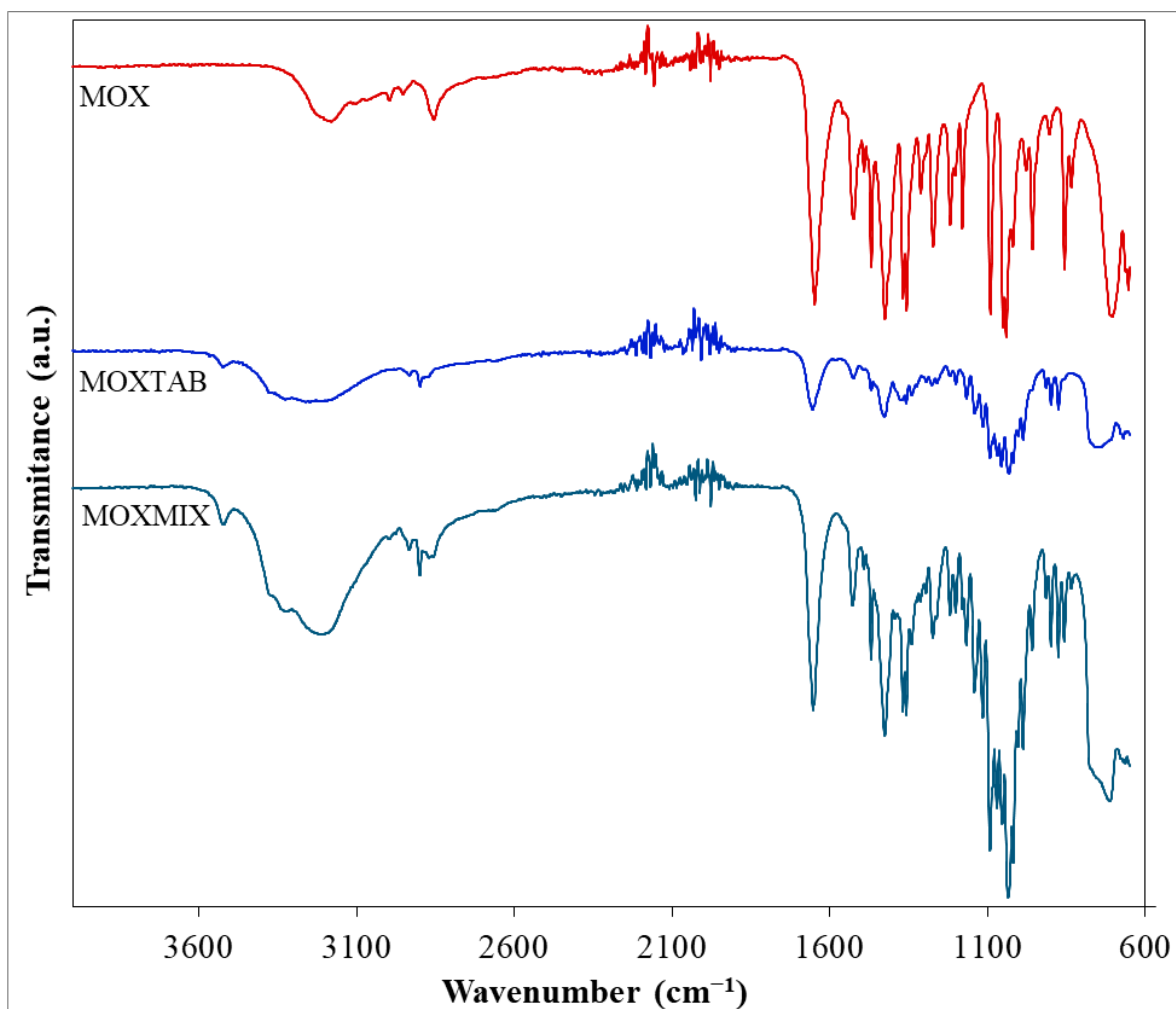


Figure 2. FTIR spectra for MOX, MOXTAB, and MOXMIX.

The spectral profiles of MOXTAB and MOXMIX are more complex due to the presence of the excipients in the analyzed mixtures (hydrated lactose, povidone K25, crospovidone, and magnesium stearate). When the spectrum of the pharmaceutical formulation MOXTAB is analyzed, it can be seen that the signals associated with MOX are attenuated in intensity and several bands that can be correlated with the presence of the excipients are revealed. For example, the stretching vibration of the O–H bonds found in the structure of lactose determines a broad band in the $3450\text{--}2990\text{ cm}^{-1}$ spectral range and a peak at 3524 cm^{-1} , while the well-defined peak seen at 1655 cm^{-1} characterizes the stretching vibration of the C=O bonds present in the structure of the other three excipients. However, the addition of MOX to MOXTAB in the sample MOXMIX is revealed, since in this sample, more bands that characterize pure MOX can be observed and the intensity of the obtained signals is significantly increased.

3.2. Thermoanalytical Investigations

The thermal stability of MOX was investigated along with MOXTAB and MOXMIX under similar conditions, and the thermoanalytical data obtained at a heating rate of $10\text{ }^{\circ}\text{C}/\text{min}$ are shown in Figures 3–5.

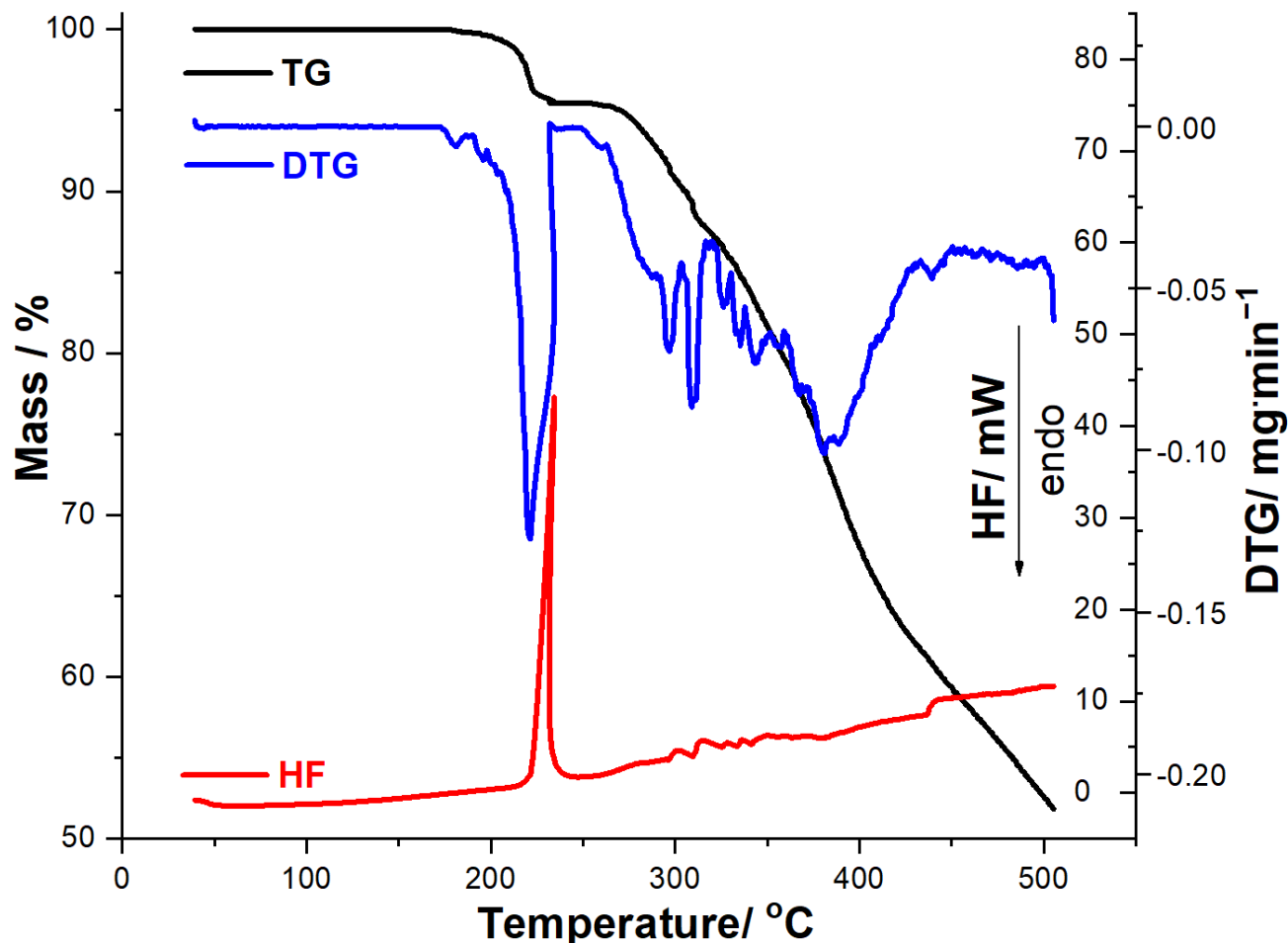


Figure 3. Thermoanalytical data (TG/DTG/HF) recorded for MOX in dynamic air atmosphere at $\beta = 10\text{ }^{\circ}\text{C}\cdot\text{min}^{-1}$.

The obtained thermoanalytical results suggest that MOX shows good thermal stability, so no mass loss or thermal events are observed under heating up to $173\text{ }^{\circ}\text{C}$, when the decomposition begins. In the $173\text{--}500\text{ }^{\circ}\text{C}$ range, MOX is degraded by a complex mechanism consisting of several consecutive steps, separated solely on the DTG curve, the residual mass being 52.25%. HF data reveal that the compound does not present an endothermic phase transition (melting), as an intense exothermic event is observed in the $221\text{--}239\text{ }^{\circ}\text{C}$ range (HF peak at $234\text{ }^{\circ}\text{C}$), while the following melting point/decomposition temperature ranges of MOX are reported in the literature: $197\text{--}205\text{ }^{\circ}\text{C}$ on Pubchem and DrugBank [49,50] and $217\text{--}225\text{ }^{\circ}\text{C}$ on AKSci [51].

In the case of solid formulation (tablet, MOXTAB), the thermoanalytical data presented in Figure 4 reveal a different behavior under thermal treatment, including a more complex HF profile, since the thermal events are associated along the API with the excipients. In the temperature range $40\text{--}159\text{ }^{\circ}\text{C}$, thermoanalytical data reveal two consecutive dehydration processes: first is the release of superficially adsorbed water (TG process between 40 and $86\text{ }^{\circ}\text{C}$, DTG_{peak} at $83\text{ }^{\circ}\text{C}$, $\Delta m_1 = 0.27\%$), followed by the dehydration of excipients, mainly hydrated lactose (TG process between 86 and $149\text{ }^{\circ}\text{C}$, DTG process between 86 and $149\text{ }^{\circ}\text{C}$, DTG_{peak} at $144\text{ }^{\circ}\text{C}$, $\Delta m_2 = 4.83\%$, HF peaks at $146\text{ }^{\circ}\text{C}$ and $147\text{ }^{\circ}\text{C}$). At temperatures over $149\text{ }^{\circ}\text{C}$, the TG curve reveals that the tablet maintains its mass in the temperature range

149–174 °C, while in the 174–214 °C interval, the third mass loss is observed ($\Delta m_3 = 2.36\%$, DTG_{peak} at 209 °C, HF_{peak} at 173 °C and 214 °C). Two well-individualized degradation processes are separated on the DTG curve: one between 214 and 258 °C ($\Delta m_4 = 15.38\%$, DTG_{peak} at 235 °C, HF_{peak} at 224 °C and 233 °C), followed by another one in the 258–331 °C interval ($\Delta m_5 = 35.07\%$, DTG_{peak} at 297 °C). At temperatures above 331 °C, thermolysis is rapid and intensely exothermic (HF peaks at 361 °C and 503 °C, respectively), resulting in a residual mass of 8.82%.

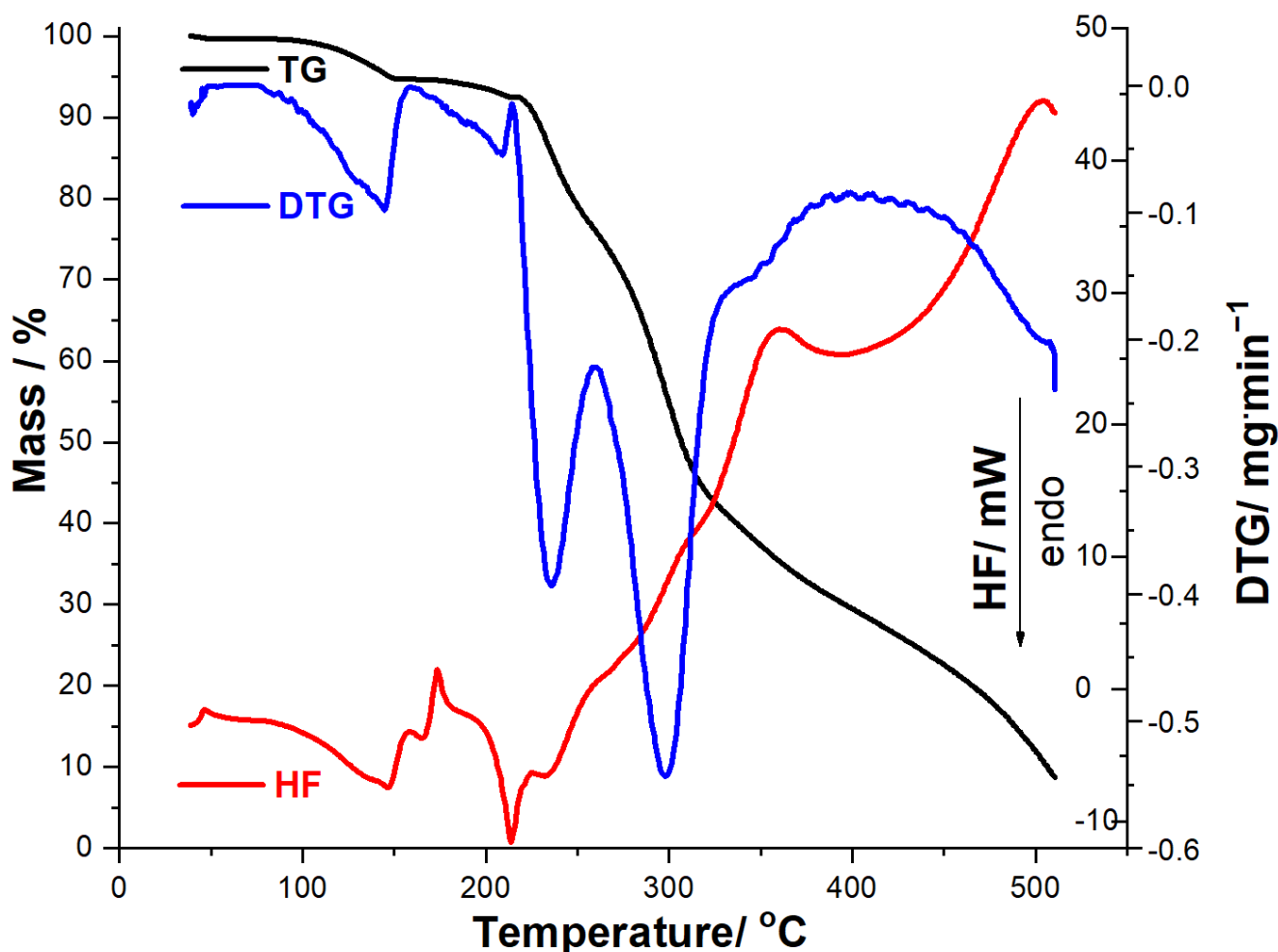


Figure 4. Thermoanalytical data (TG/DTG/HF) recorded for MOXTAB in dynamic air atmosphere at $\beta = 10\text{ }^{\circ}\text{C}\cdot\text{min}^{-1}$.

Thermoanalytical data (TG/DTG/HF) recorded for MOXMIX in dynamic air atmosphere at $\beta = 10\text{ }^{\circ}\text{C}\cdot\text{min}^{-1}$ (Figure 5) are closer to the MOX profile, since it contains a significantly higher amount of API compared to MOXTAB. TG data reveal that this sample is thermally stable up to 88 °C, when the first mass loss occurs up to 146 °C, i.e., a dehydration that is also evidenced by DTG_{peaks} at 88 °C and 127 °C and HF_{peak} at 129 °C, with a corresponding mass loss $\Delta m_1 = 4.44\%$. MOXMIX is then thermally stable, and no mass loss occurs between 146 and 168 °C, followed at 168–500 °C by a continuous mass loss due to thermolysis. On the DTG curve, there is a well-individualized mass loss process in the 168–242 °C range, with two overlapped DTG_{peaks} at 199 °C and 203 °C, HF_{peaks} at 172 °C, 191 °C, and 230 °C, and a corresponding mass loss $\Delta m_2 = 34.15\%$. At temperatures over 242 °C, thermolysis leads to a final residual mass of 14.55%, which is greater than the one obtained when the MOXTAB sample was analyzed. This behavior can be explained by the supplementary quantity of API, which has a greater residual mass at 500 °C compared to the excipients.

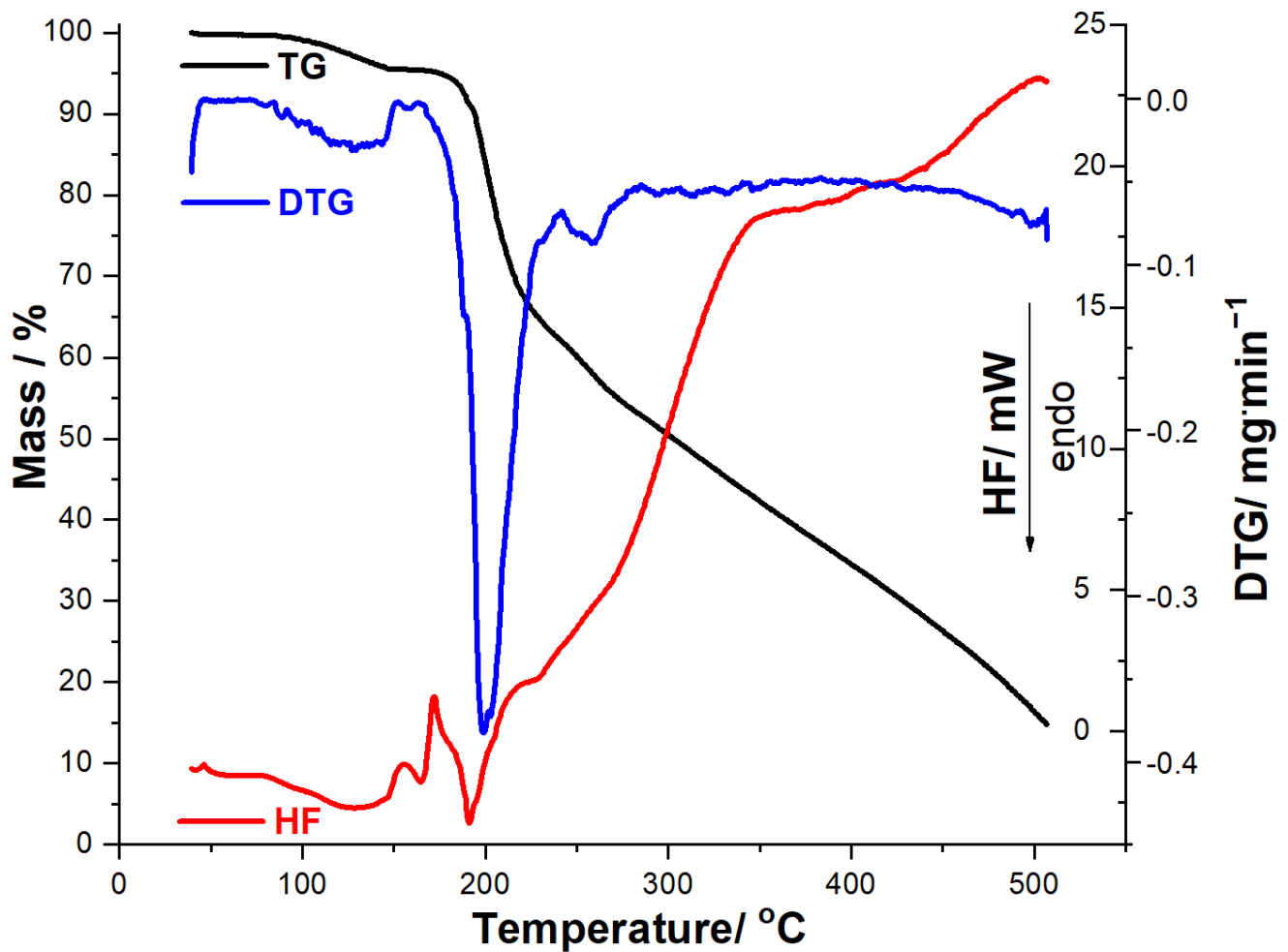


Figure 5. Thermoanalytical data (TG/DTG/HF) recorded for MOXMIX in dynamic air atmosphere at $\beta = 10 \text{ }^\circ\text{C}\cdot\text{min}^{-1}$.

3.3. Kinetic Study

The aim of this kinetic study was to evaluate the effect of the excipient on MOX degradation. Since the thermal degradation of MOX is a heterogenous solid-state process, Equation (1) describes the reaction rate in differential form, where:

$$\beta \frac{d\alpha}{dT} = A \cdot f(\alpha) \cdot \exp\left(-\frac{E_a}{RT}\right) \quad (1)$$

Equation (2) describes the reaction rate in integral form, after the integration of differential Equation (1) with the separation of variables for α belonging to the $[0, \alpha]$ interval and T belonging to the $[T_0, T]$ interval, where T_0 represents the temperature at which the investigated process begins:

$$g(\alpha) = \int_0^\alpha \frac{d\alpha}{f(\alpha)} = \frac{A}{\beta} \int_{T_0}^T \left[\exp\left(-\frac{E_a}{RT}\right) \right] dT \quad (2)$$

The fraction of mass loss (i.e., the degree of conversion) can be calculated using Equation (3):

$$\alpha_{(T)} = \frac{m_0 - m_T}{m_0 - m_f} \quad (3)$$

According to the ICTAC protocols, the use of model-free isoconversional methods is recommended over model-fitting methods, and the integral methods of FWO and Kissinger–

Akahira–Sunose and the FR differential method are by far the most frequently utilized methods for the kinetic analysis of solid-state degradation processes [28].

The decomposition kinetics was estimated from the TG/DTG curvatures using the ASTM E698 method [52,53] as a preliminary investigational method, followed by the employment of two isoconversional methods, namely, the FR differential method [54] and the integral method of FWO [55,56]. The advantages and limitations of isoconversional methods, as well as their development and use over time, are reported exhaustively in the literature [57–59]. However, to facilitate the access to information of the readers, a brief presentation of the mathematical models of the isoconversional methods is shown in Table 1.

Table 1. Mathematical models of the integral method of FWO and the differential method of FR.

| Method | Linearized Form | Plotting |
|--------|---|---|
| FWO | $\ln \beta = \ln \frac{A \cdot E_a}{R \cdot g(\alpha)} - 5.331 - \frac{1.052 \cdot E_a}{R \cdot T}$ | $\ln \beta$ vs. $(1/T)$ |
| FR | $\ln \left(\beta \frac{d\alpha}{dT} \right) = \ln [A \cdot f(\alpha)] - \frac{E_a}{R \cdot T}$ | $\ln \left(\beta \frac{d\alpha}{dT} \right)$ vs. $(1/T)$ |

The kinetically investigated degradation process was selected based on the aspect of the TG/DTG/HF curves for MOX, and the same process was chosen for both the pharmaceutical form (MOXTAB) and the MOX-enriched sample mixture (MOXMIX), according to the DTG curves. For the analyzed samples, the degradation process that was investigated from the kinetic point of view was chosen based on the aspect of the DTG curves for each heating rate, and the temperature intervals are presented in Table 2.

Table 2. Temperature interval according to DTG curves for the degradation process that was investigated by kinetic analysis.

| Heating Rate β (°C·min ⁻¹) | DTG Temperature Interval (°C) for Kinetic Analysis of Samples | | |
|---|---|---------|---------|
| | MOX | MOXTAB | MOXMIX |
| 5 | 174–244 | 187–243 | 150–227 |
| 7 | 175–247 | 190–248 | 154–231 |
| 10 | 175–253 | 193–254 | 165–241 |
| 15 | 176–260 | 199–259 | 168–243 |

The results obtained after performing the ASTM E698 kinetic study are presented in Figure 6a–c.

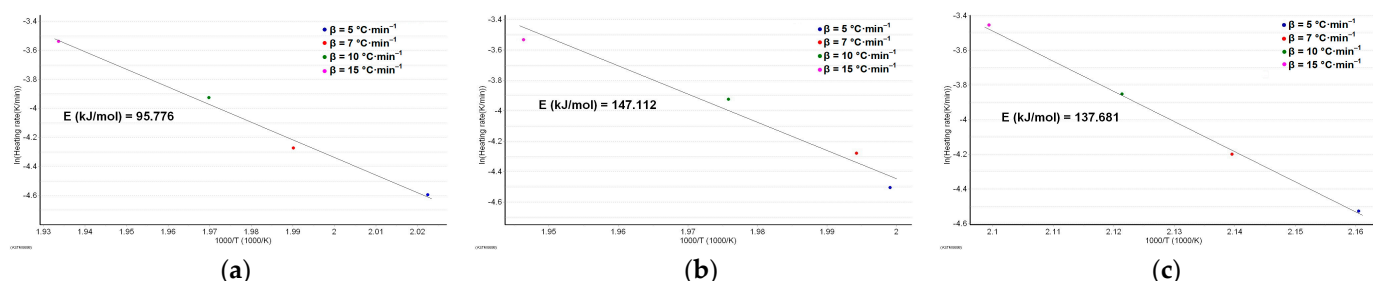


Figure 6. The plot according to the ASTM E698 kinetic method with the estimated activation energy for: (a) MOX; (b) MOXTAB; and (c) MOXMIX.

As can be seen in Figure 6a–c, the variation in activation energy using the DTG peaks at the selected heating rates is significant. The preliminary information provided by this method is that the stability of MOX (in terms of activation energy, E_a for MOX being $95.8 \text{ kJ} \cdot \text{mol}^{-1}$) seems to increase in the presence of excipients from formulation, and the

degradation process requires an additional 53% energy for the degradation of the tablet (E_a for MOXTAB is $147.1 \text{ kJ}\cdot\text{mol}^{-1}$). The destabilizing effect of moxonidine in the mixture is also proven after the analysis of the MOXMIX model system: the presence of the additional mass of active ingredient determines a decrease in activation energy to $137.7 \text{ kJ}\cdot\text{mol}^{-1}$.

The reaction progress was analyzed for all three samples, and the results obtained are presented in Figure S1a–c. Additionally, the increase in reaction rate and the shift in its maximum to higher temperatures with the increase in heating rate due to thermal inertia was observed for all three analyzed samples, as seen in Figure S2a–c, in good agreement with the reaction progress presented in Figure S1a–c.

The isoconversional kinetic study according to the FWO method was carried out by estimating the activation energy values vs. α for each heating rate, from the slopes of the linear plots of $\ln\beta$ vs. T^{-1} , as seen in Figure S3, with the corresponding values presented in Table 3. The obtained values agree with the results obtained by the ASTM E698 method, increasing to 5.84% for MOX, 18.1% for MOXTAB, and 1.81% for MOXMIX. Similarly, using the FR method, the plot of $\ln(\beta \cdot d\alpha/dT)$ vs. T^{-1} is linear (Figure S4), and the individual $E_a(\alpha)$ values were estimated for the same conversion degrees as in the case of the FWO method (Table 2).

Table 3. E_a values vs. conversion degree α obtained by the two isoconversional methods and the mean value of E_a for MOX, MOXTAB, and MOXMIX.

| Compound | α | 0.05 | 0.1 | 0.15 | 0.2 | 0.25 | 0.3 | 0.35 | 0.4 | 0.45 | 0.5 | 0.55 | 0.6 | 0.65 | 0.7 | 0.75 | 0.8 | 0.85 | 0.9 | 0.95 | $\overline{E_a}$ ($\text{kJ}\cdot\text{mol}^{-1}$) |
|----------|----------|-------|-------|-------|-------|-------|-------|-------|-------|-------|-------|-------|-------|-------|-------|-------|-------|-------|-------|-------|---|
| MOX | FWO | 98.8 | 102.8 | 103.4 | 103.5 | 103.3 | 103.0 | 102.6 | 102.1 | 101.6 | 101.2 | 100.8 | 100.6 | 100.3 | 100.0 | 99.6 | 99.3 | 99.1 | 98.9 | 106.4 | 101.4 ± 0.5 |
| | FR | 127.7 | 118.2 | 106.9 | 95.2 | 92.6 | 89.3 | 86.6 | 85.1 | 84.5 | 84.0 | 83.6 | 82.4 | 81.3 | 80.8 | 81.3 | 87.5 | 94.6 | 100.6 | 115.2 | 93.6 ± 3.2 |
| MOXTAB | FWO | 201.0 | 185.9 | 180.1 | 179.2 | 173.2 | 186.7 | 181.8 | 178.2 | 174.8 | 171.8 | 170.0 | 168.9 | 167.3 | 165.3 | 164.4 | 163.2 | 162.6 | 163.7 | 163.1 | 173.7 ± 2.4 |
| | FR | 164.1 | 113.7 | 133.8 | 144.8 | 148.1 | 139.1 | 143.9 | 146.1 | 143.4 | 144.3 | 159.9 | 157.3 | 150.0 | 140.9 | 162.1 | 152.2 | 161.5 | 164.6 | 167.3 | 149.3 ± 3.0 |
| MOXMIX | FWO | 141.6 | 143.3 | 142.7 | 147.0 | 152.0 | 151.7 | 150.4 | 149.3 | 148.1 | 147.0 | 146.0 | 145.0 | 143.5 | 142.5 | 141.5 | 137.6 | 133.8 | 132.2 | 129.6 | 143.4 ± 1.5 |
| | FR | 164.7 | 126.1 | 157.1 | 154.0 | 157.1 | 144.5 | 137.7 | 137.9 | 137.7 | 136.6 | 138.1 | 134.5 | 131.1 | 140.9 | 112.4 | 97.6 | 122.1 | 121.8 | 121.2 | 135.4 ± 3.8 |

The analysis of variation in E_a vs. α using such a narrow variation for conversion (5%) allows the estimation of a medium value of activation energy for the whole investigated process (considered a single-step process), but only if the variation in individual E_a values is placed inside a confidence interval of $\pm 10\%$ around the calculated medium value, i.e., $0.9 \cdot \overline{E_a} \leq E_a(\alpha) \leq 1.1 \cdot \overline{E_a}$. As a consequence, if the variation in $E_a(\alpha)$ is monotonous (increasing or decreasing) or arbitrary, a multi-step degradation process, or a modification of the mechanism with increasing heating rate, is suspected (Figure S5).

The analysis of the data presented in Table 3 and Figure S5a–c reveals that the integral processing of the kinetic data according to the FWO isoconversional method indicates that the degradation of all samples is characterized by a mechanism that is not dependent on the degree of conversion, when $0.1 \leq \alpha \leq 0.95$. In the case of MOXTAB, there is solely one value for E_a outside the confidence interval, at $\alpha = 5\%$. For all samples, the tendency for E_a values follows different trends (Figure S5a–c) up to $\alpha = 0.25$ and for $\alpha > 0.3$, suggesting the existence of complex degradation processes. This tendency is more evident for MOXTAB and MOXMIX, where the presence of excipients is the reason for this behavior.

The FR isoconversional method (Figure S5d–f) reveals a higher dispersion of the E_a values vs. α outside the $\pm 10\%$ limit. For MOX, the E_a values are higher at the beginning of the process, at lower conversion degrees ($\alpha < 0.2$), and at the end of the process ($\alpha > 0.85$). Furthermore, for MOXTAB and MOXMIX, the variation in E_a vs. α is irregular, mostly with extreme values for MOXMIX at $\alpha < 0.25$, suggesting a complex mechanism of decomposition of these samples under thermal stress.

4. Conclusions

In this paper, we present the findings of the instrumental screening of the drug moxonidine, both as a pure ingredient and also in the presence of several excipients that

are currently used in a commercial solid formulation that contains 0.4 mg API per tablet. To evaluate the excipient effect, we prepared an enriched mixture starting from this commercial formulation by adding pure API until a 5:1 tablet/API ratio was achieved. All samples were characterized by FTIR spectroscopy in order to check the identity and purity of MOX and to confirm the presence of API in the tablet and in the mixture. Thermal investigations were carried out for all samples using a dynamic oxidative atmosphere and four different linear heating rates, and the obtained data were processed using three kinetic methods. Initially, the simple ASTM-E698 method was used, and later, the isoconversional methods of FWO and FR were employed. If used alone, the ASTM-E698 method cannot produce realistic kinetic parameters regarding reactions that include simultaneous or consecutive reaction steps, while the isoconversional methods allow an estimation of the values of E_a vs. conversion degree. The different results of the three methods reside in the mathematical processing of the data, since in the case of the ASTM E698 method, the estimated E_a value does not consider the conversion degree as it is a mean value for the entirely investigated process. Excipients showed a stabilizing effect on MOX (in terms of E_a values), but the decomposition mechanism of the samples is complex, according to the results suggested by the analysis of E_a vs. α values.

Supplementary Materials: The following supporting information can be downloaded at: <https://www.mdpi.com/article/10.3390/pr11061738/s1>, Figure S1: The reaction progress vs. temperature at selected heating rates for: (a) MOX; (b) MOXTAB; and (c) MOXMIX. Figure S2: The reaction rate vs. temperature at selected heating rates for: (a) MOX; (b) MOXTAB; and (c) MOXMIX. Figure S3: Linear plot of FWO integral isoconversional method of the analyzed decomposition process for: (a) MOX; (b) MOXTAB; and (c) MOXMIX. Figure S4: Linear plotting of FR differential isoconversional method of the analyzed process of decomposition for: (a) MOX; (b) MOXTAB; and (c) MOXMIX. Figure S5: Variation in E_a vs. α according to FWO integral isoconversional method (a–c) and FR differential isoconversional method (d–f) of the analyzed decomposition process for: (a,d) MOX; (b,e) MOXTAB; and (c,f) MOXMIX.

Author Contributions: Conceptualization, B.B., A.L. and I.L.; methodology, B.B., D.C., T.V., G.V. and A.L.; validation, I.L., F.P., and T.V.; investigation, B.B., A.R. and D.C.; resources, A.L., F.P., T.V., G.V. and I.L.; writing—original draft preparation, I.L., D.C., A.L., G.V. and B.B.; writing—review and editing, A.L., F.P., D.C. and I.L.; supervision, A.L., T.V., F.P. and I.L.; project administration, B.B. All authors have read and agreed to the published version of the manuscript.

Funding: This paper was financially supported by the Project “Network of excellence in applied research and innovation for doctoral and postdoctoral programs/InoHubDoc”, project co-funded by the European Social Fund financing agreement no. POCU/993/6/13/153437.

Data Availability Statement: Raw data are available from the corresponding author of this work, on request.

Conflicts of Interest: The authors declare that they have no known competing financial interests or personal relationships that could have appeared to influence the work reported in this paper.

References

1. Gamboa, A.; Okamoto, L.E.; Shibao, C.A.; Biaggioni, I. Obesity-associated hypertension. In *Primer on the Autonomic Nervous System*; Biaggioni, I., Browning, K., Fink, G., Jordan, J., Low, P.A., Paton, J.F.R., Eds.; Academic Press: Cambridge, MA, USA, 2023; pp. 471–474, ISBN 978-0-323-85492-4.
2. Karlafti, E.; Didangelos, T.; Benioudakis, E.; Kotzakioulafi, E.; Kaiafa, G.; Kotsis, V.; Ziakas, A.; Doumas, M.; Goulas, A.; Savopoulos, C. Effects of Moxonidine Administration on Serum Neuropeptide Y Levels in Hypertensive Individuals: A Prospective Observational Study. *Endocrines* **2022**, *3*, 43–52. [[CrossRef](#)]
3. Karlafti, E.F.; Hatzitoliou, A.I.; Karlaftis, A.F.; Baltatzi, M.S.; Koliakos, G.G.; Savopoulos, C.G. Effects of moxonidine on sympathetic nervous system activity: An update on metabolism, cardio, and other target-organ protection. *J. Pharm. Bioallied Sci.* **2013**, *5*, 253–256. [[PubMed](#)]
4. Fenton, C.; Keating, G.M.; Lyseng-Williamson, K.A. Moxonidine: A review of its use in essential hypertension. *Drugs* **2006**, *66*, 477–496. [[CrossRef](#)] [[PubMed](#)]

5. Abellán, J.; Leal, M.; Hernández-Menárguez, F.; García-Galbis, J.A.; Martínez-Pastor, A.; De Vinuesa, S.G.; Luño, J. Efficacy of moxonidine in the treatment of hypertension in obese, noncontrolled hypertensive patients. *Kidney Int. Suppl.* **2005**, *67*, S20–S24. [[CrossRef](#)] [[PubMed](#)]
6. Wang, Y.; Nguyen, D.T.; Anesi, J.; Alramahi, A.; Witting, P.K.; Chai, Z.; Khan, A.W.; Kelly, J.; Denton, K.M.; Golledge, J. Moxonidine Increases Uptake of Oxidised Low-Density Lipoprotein in Cultured Vascular Smooth Muscle Cells and Inhibits Atherosclerosis in Apolipoprotein E-Deficient Mice. *Int. J. Mol. Sci.* **2023**, *24*, 3857. [[CrossRef](#)] [[PubMed](#)]
7. Ernsberger, P.; Friedman, J.E.; Koletsky, R.J. The I1-imidazoline receptor. *J. Hypertens.* **1997**, *15*, S9–S23. [[CrossRef](#)]
8. Sveinsdóttir, H.S.; Christensen, C.; Þorsteinsson, H.; Lavalou, P.; Parker, M.O.; Shkumatava, A.; Norton, W.H.J.; Andriambeloson, E.; Wagner, S.; Karlsson, K.Æ. Novel non-stimulants rescue hyperactive phenotype in an adgrl3.1 mutant zebrafish model of ADHD. *Neuropsychopharmacology* **2022**. [[CrossRef](#)]
9. Kramzer, L.F.; Hamorsky, K.T.; Graebing, P.W.; Wang, L.; Fuqua, J.L.; Matoba, N.; Lasnik, A.B.; Moncla, B.J.; Zhang, J.; Palmer, K.E.; et al. Preformulation Characterization of Griffithsin, a Biopharmaceutical Candidate for HIV Prevention. *AAPS PharmSciTech* **2021**, *22*, 83. [[CrossRef](#)]
10. Asran, A.M.; Mohamed, M.A.; Khedr, G.E.; Eldin, G.M.G.; Yehia, A.M.; Mishra, R.K.; Allam, N.K. Investigation of the thermal stability of the antihypertensive drug nebivolol under different conditions: Experimental and computational analysis. *J. Therm. Anal. Calorim.* **2022**, *147*, 5779–5786. [[CrossRef](#)]
11. Bengescu, C.; Ledeti, A.; Olariu, T.; Cîrcioaban, D.; Muntean, C.; Vlase, G.; Vlase, T.; Tomoroga, C.; Dragomirescu, A.O.; Dascălu, D.; et al. Instrumental investigations of promestriene: First report regarding the solid-state characterization and compatibility with pharmaceutical excipients. *J. Therm. Anal. Calorim.* **2023**, *148*, 4641–4649. [[CrossRef](#)]
12. Ledeti, I.; Bolintineanu, S.; Vlase, G.; Cîrcioaban, D.; Ledeti, A.; Vlase, T.; Suta, L.M.; Caunii, A.; Murariu, M. Compatibility study between antiparkinsonian drug Levodopa and excipients by FTIR spectroscopy, X-ray diffraction and thermal analysis. *J. Therm. Anal. Calorim.* **2017**, *130*, 433–441. [[CrossRef](#)]
13. Rojek, B.; Wesolowski, M. A combined differential scanning calorimetry and thermogravimetry approach for the effective assessment of drug substance-excipient compatibility. *J. Therm. Anal. Calorim.* **2023**, *148*, 845–858. [[CrossRef](#)]
14. Li, X.; Liu, J.; Qiu, N. Cyclodextrin-Based Polymeric Drug Delivery Systems for Cancer Therapy. *Polymers* **2023**, *15*, 1400. [[CrossRef](#)] [[PubMed](#)]
15. Kovacs, T.; Nagy, P.; Panyi, G.; Szente, L.; Varga, Z.; Zakany, F. Cyclodextrins: Only Pharmaceutical Excipients or Full-Fledged Drug Candidates? *Pharmaceutics* **2022**, *14*, 2559. [[CrossRef](#)] [[PubMed](#)]
16. Soe, H.M.S.H.; Maw, P.D.; Loftsson, T.; Jansook, P. A Current Overview of Cyclodextrin-Based Nanocarriers for Enhanced Antifungal Delivery. *Pharmaceutics* **2022**, *15*, 1447. [[CrossRef](#)]
17. De Gaetano, F.; Cristiano, M.C.; Paolino, D.; Celesti, C.; Iannazzo, D.; Pistarà, V.; Iraci, N.; Ventura, C.A. Bicalutamide Anticancer Activity Enhancement by Formulation of Soluble Inclusion Complexes with Cyclodextrins. *Biomolecules* **2022**, *12*, 1716. [[CrossRef](#)]
18. Dhondale, M.R.; Thakor, P.; Nambiar, A.G.; Singh, M.; Agrawal, A.K.; Shastri, N.R.; Kumar, D. Co-Crystallization Approach to Enhance the Stability of Moisture-Sensitive Drugs. *Pharmaceutics* **2023**, *15*, 189. [[CrossRef](#)]
19. Xie, Y.; Yuan, P.; Heng, T.; Du, L.; An, Q.; Zhang, B.; Zhang, L.; Yang, D.; Du, G.; Lu, Y. Insight into the Formation of Cocrystal and Salt of Tenoxicam from the Isomer and Conformation. *Pharmaceutics* **2022**, *14*, 1968. [[CrossRef](#)]
20. Birolo, R.; Bravetti, F.; Bordignon, S.; D’Abbrunzo, I.; Mazzeo, P.P.; Perissutti, B.; Bacchi, A.; Chierotti, M.R.; Gobetto, R. Overcoming the Drawbacks of Sulpiride by Means of New Crystal Forms. *Pharmaceutics* **2022**, *14*, 1754. [[CrossRef](#)]
21. Islam, N.U.; Umar, M.N.; Khan, E.; Al-Joufi, F.A.; Abed, S.N.; Said, M.; Ullah, H.; Iftikhar, M.; Zahoor, M.; Khan, F.A. Levofloxacin Cocrystal/Salt with Phthalimide and Caffeic Acid as Promising Solid-State Approach to Improve Antimicrobial Efficiency. *Antibiotics* **2022**, *11*, 797. [[CrossRef](#)]
22. Drozd, K.V.; Manin, A.N.; Boycov, D.E.; Perlovich, G.L. Simultaneous Improvement of Dissolution Behavior and Oral Bioavailability of Antifungal Miconazole via Cocrystal and Salt Formation. *Pharmaceutics* **2022**, *14*, 1107. [[CrossRef](#)] [[PubMed](#)]
23. Mateescu, M.; Vlase, G.; Budiul, M.M.; Cernuşcă, B.D.; Vlase, T. Preliminary study for preparation and characterization of medicated jelly based on Ibuprofen or Ambroxol. *J. Therm. Anal. Calorim.* **2023**, *148*, 4601–4614. [[CrossRef](#)]
24. Aslam, A.; Ashraf, M.U.; Barkat, K.; Mahmood, A.; Hussain, M.A.; Farid-ul-Haq, M.; Lashkar, M.O.; Gad, H.A. Fabrication of Stimuli-Responsive Quince/Mucin Co-Poly (Methacrylate) Hydrogel Matrices for the Controlled Delivery of Acyclovir Sodium: Design, Characterization and Toxicity Evaluation. *Pharmaceutics* **2023**, *15*, 650. [[CrossRef](#)]
25. Vecchio, S.; Rodante, F.; Tomassetti, M. Thermal stability of disodium and calcium phosphomycin and the effects of the excipients evaluated by thermal analysis. *J. Pharm. Biomed. Anal.* **2001**, *24*, 1111–1123. [[CrossRef](#)] [[PubMed](#)]
26. Chachorovska, M.; Petrushevski, G.; Stojanovska Pecova, M.; Ugarkovic, S.; Makreski, P. Thermal analysis assisted by spectrostructure studies of BCS class II active pharmaceutical ingredients: Ezetimibe and lercanidipine hydrochloride. The concept of preformulation. *J. Therm. Anal. Calorim.* **2022**, *147*, 8779–8790. [[CrossRef](#)]
27. Ledeti, A.; Olariu, T.; Caunii, A.; Vlase, G.; Cîrcioaban, D.; Baul, B.; Ledeti, I.; Vlase, T.; Murariu, M. Evaluation of thermal stability and kinetic of degradation for levodopa in non-isothermal conditions. *J. Therm. Anal. Calorim.* **2018**, *131*, 1881–1888. [[CrossRef](#)]
28. Kremer, I.; Tomić, T.; Katančić, Z.; Hrnjak-murgić, Z.; Erceg, M.; Cipriotti, S.V.; Schneider, D.R. Effect of Zeolite Catalyst on the Pyrolysis Kinetics of Multi-Layered Plastic Food Packaging. *Symmetry* **2022**, *14*, 1362. [[CrossRef](#)]
29. Arcenegui-Troya, J.; Sánchez-Jiménez, P.E.; Perejón, A.; Pérez-Maqueda, L.A. Relevance of particle size distribution to kinetic analysis: The case of thermal dehydroxylation of kaolinite. *Processes* **2021**, *9*, 1852. [[CrossRef](#)]

30. Rotaru, A.; Moanta, A.; Constantinescu, C.; Dumitru, M.; Manolea, H.O.; Andrei, A.; Dinescu, M. Thermokinetic study of CODA azoic liquid crystal and thin films deposition by matrix-assisted pulsed laser evaporation. *J. Therm. Anal. Calorim.* **2017**, *128*, 89–105. [CrossRef]
31. Brown, M.E.; Maciejewski, M.; Vyazovkin, S.; Nomen, R.; Sempere, J.; Burnham, A.; Opfermann, J.; Strey, R.; Anderson, H.L.; Kemmler, A.; et al. Computational aspects of kinetic analysis Part A: The ICTAC Kinetics Project-data, methods and results. *Thermochim. Acta* **2000**, *355*, 125–143. [CrossRef]
32. Vyazovkin, S. Computational aspects of kinetic analysis. Part C. The ICTAC Kinetics Project—The light at the end of the tunnel? *Thermochim. Acta* **2000**, *355*, 155–163. [CrossRef]
33. Roduit, B. Computational aspects of kinetic analysis. Part E: The ICTAC Kinetics Project—Numerical techniques and kinetics of solid state processes. *Thermochim. Acta* **2000**, *355*, 171–180. [CrossRef]
34. Verma, R.K.; Szilagyi, I.M.; Pielichowska, K.; Raftopoulos, K.N.; Šimon, P.; Melnikov, A.P.; Ivanov, D.A. Good laboratory practice in thermal analysis and calorimetry. *J. Therm. Anal. Calorim.* **2023**, *148*, 2211–2231. [CrossRef]
35. Zou, H.; Yi, C.; Wang, L.; Liu, H.; Xu, W. Thermal degradation of poly(lactic acid) measured by thermogravimetry coupled to Fourier transform infrared spectroscopy. *J. Therm. Anal. Calorim.* **2009**, *97*, 929–935. [CrossRef]
36. Pal, A.K.; Katiyar, V. Theoretical and analyzed data related to thermal degradation kinetics of poly (L-lactic acid)/chitosan-grafted-oligo L-lactic acid (PLA/CH-g-OLLA) bionanocomposite films. *Data Br.* **2017**, *10*, 304–311. [CrossRef]
37. Guigo, N.; Sbirrazzuoli, N.; Vyazovkin, S. Gelation on heating of supercooled gelatin solutions. *Macromol. Rapid Commun.* **2012**, *33*, 698–702. [CrossRef]
38. Zhao, L.; Ding, L.; Wei, X. Determination of moxonidine in human plasma by liquid chromatography- electrospray ionisation-mass spectrometry. *J. Pharm. Biomed. Anal.* **2006**, *40*, 95–99. [CrossRef]
39. Zhang, Q.; Chu, M.F.; Li, Y.H.; Li, C.H.; Lei, R.J.; Wang, S.C.; Xiao, B.J.; Yang, J.G. Quantitative analysis by reversed-phase high-performance liquid chromatography and retinal neuroprotection after topical administration of moxonidine. *Int. J. Ophthalmol.* **2020**, *13*, 390–398. [CrossRef]
40. Filipic, S.; Shenger, M.S.M.; Nikolic, K.; Agbaba, D. Determination of Moxonidine and Its Impurities by Thin-Layer Chromatography. *J. Liq. Chromatogr. Relat. Technol.* **2015**, *38*, 1121–1125. [CrossRef]
41. Otašević, B.; Milovanović, S.; Zečević, M.; Golubović, J.; Protić, A. UPLC method for determination of moxonidine and its degradation products in active pharmaceutical ingredient and pharmaceutical dosage form. *Chromatographia* **2014**, *77*, 109–118. [CrossRef]
42. Milovanović, S.; Otašević, B.; Zečević, M.; Živanović, L.; Protić, A. Development and validation of reversed phase high performance liquid chromatographic method for determination of moxonidine in the presence of its impurities. *J. Pharm. Biomed. Anal.* **2012**, *59*, 151–156. [CrossRef] [PubMed]
43. Filipic, S.; Elek, M.; Popović, M.; Nikolic, K.; Agbaba, D. Development of Hydrophilic Interaction Liquid Chromatography Method for the Analysis of Moxonidine and Its Impurities. *J. Anal. Methods Chem.* **2016**, *2016*, 3715972. [CrossRef] [PubMed]
44. Allada, R.; Maruthapillai, A.; Devikala, S.; Pallepogu, R. Hydrated moxonidine saccharinatesalt: Synthesis, Characterization, Crystal structure determination and dissolution enhancement. *Mater. Today Proc.* **2019**, *14*, 618–629. [CrossRef]
45. Vyazovkin, S.; Achilias, D.; Fernandez-Francos, X.; Galukhin, A.; Sbirrazzuoli, N. ICTAC Kinetics Committee recommendations for analysis of thermal polymerization kinetics. *Thermochim. Acta* **2022**, *714*, 179243. [CrossRef]
46. Stuart, B.H. *Infrared Spectroscopy: Fundamentals and Applications*; John Wiley & Sons: Hoboken, NJ, USA, 2004; ISBN 0470011130.
47. Silverstein, R.M.; Webster, F.X.; Kiemle, D. *Spectrometric Identification of Organic Compounds*, 7th ed.; John Wiley & Sons: Hoboken, NJ, USA, 2005; ISBN 9781118311653.
48. Coates, J. Interpretation of Infrared Spectra, A Practical Approach. In *Encyclopedia of Analytical Chemistry*; Meyers, R.A., McKelvy, M.L., Eds.; John Wiley & Sons: Hoboken, NJ, USA, 2006; ISBN 9780470027318. [CrossRef]
49. Moxonidine (Compound) on PubChem. Available online: <https://pubchem.ncbi.nlm.nih.gov/compound/Moxonidine#section=Melting-Point> (accessed on 22 March 2023).
50. Moxonidine (Compound) on DrugBank. Available online: <https://go.drugbank.com/drugs/DB09242> (accessed on 22 March 2023).
51. Moxonidine (Compound) on AKSci. Available online: https://aksci.com/item_detail.php?cat=K289 (accessed on 22 March 2023).
52. Duswalt, A.A. The practice of obtaining kinetic data by differential scanning calorimetry. *Thermochim. Acta* **1974**, *8*, 57–68. [CrossRef]
53. Lu, W.-Y.; Lin, W.-C.; Huang, A.-C.; Shu, C.-M. Determination of the ambience duration of lavender essential oil with three perfume fixatives using the thermokinetics approach. *J. Therm. Anal. Calorim.* **2022**, *147*, 7551–7561. [CrossRef]
54. Friedman, H.L. Kinetics of thermal degradation of char-forming plastics from thermogravimetry. Application to a phenolic plastic. *J. Polym. Sci.* **1964**, *6*, 183–195. [CrossRef]
55. Flynn, J.H.; Wall, L.A. A quick, direct method for the determination of activation energy from thermogravimetric data. *J. Polym. Sci. Part B Polym. Lett.* **1966**, *4*, 323–328. [CrossRef]
56. Ozawa, T.A. New Method of Analyzing Thermogravimetric Data. *Bull. Chem. Soc. Jpn.* **1965**, *38*, 1881–1886. [CrossRef]
57. Vyazovkin, S. Isoconversional kinetics. In *Handbook of Thermal Analysis and Calorimetry, Vol. 5: Recent Advances, Techniques and Applications*; Brown, M.E., Gallagher, P.K., Eds.; Elsevier: Amsterdam, The Netherlands, 2008; pp. 503–538.

58. Budrugaec, P.; Cucos, A. Application of Kissinger, isoconversional and multivariate non-linear regression methods for evaluation of the mechanism and kinetic parameters of phase transitions of type I collagen. *Thermochim. Acta* **2013**, *565*, 241–252. [[CrossRef](#)]
59. Budrugaec, P.; Criado, J.M.; Gotor, F.J.; Malek, J.; Pérez-Maqueda, L.A.; Segal, E. On the evaluation of the nonisothermal kinetic parameters of (GeS₂)_{0.3}(Sb₂S₃)_{0.7} crystallization using the IKP method. *Int. J. Chem. Kinet.* **2004**, *36*, 309–315. [[CrossRef](#)]

Disclaimer/Publisher's Note: The statements, opinions and data contained in all publications are solely those of the individual author(s) and contributor(s) and not of MDPI and/or the editor(s). MDPI and/or the editor(s) disclaim responsibility for any injury to people or property resulting from any ideas, methods, instructions or products referred to in the content.